THE JOURNAL OF PHYSICAL CHEMISTRY C

Article

Cite This: J. Phys. Chem. C 2017, 121, 24144-24151

pubs.acs.org/JPCC

Where Is the Most Hydrophobic Region? Benzopurpurine Self-Assembly at the Calcite–Water Interface

Martin Nalbach,[†] Paolo Raiteri,*[,‡] Stefanie Klassen,[†] Sven Schäfer,[†] Julian D. Gale,[‡] Ralf Bechstein,[†] and Angelika Kühnle*[,†]

[†]Institute of Physical Chemistry, Johannes Gutenberg University Mainz, Duesbergweg 10-14, 55099 Mainz, Germany

[‡]Curtin Institute for Computation, The Institute for Geoscience Research (TIGeR) and Department of Chemistry, Curtin University, P.O. Box U1987, Perth, Western Australia 6845, Australia

Supporting Information

ABSTRACT: Control of molecular self-assembly at solid–liquid interfaces is challenging due to the complex interplay between molecule–molecule, molecule–surface, molecule–solvent, surface–solvent, and solvent–solvent interactions. Here, we use *in-situ* dynamic atomic force microscopy to study the self-assembly of Benzopurpurine 4B into oblong islands with a highly ordered inner structure yet incommensurate with the underlying calcite (10.4) surface. Molecular dynamics and free energy calculations provide insights by showing that Benzopurpurine 4B molecules do not anchor to the surface directly but instead assemble on top of the second hydration layer. This seemingly peculiar behavior was then rationalized by considering that hydrophobic molecules placed atop the second water layer cause the least distortion to the existing hydration structure. Further experiments for the adsorption of Benzopurpurine 4B on other minerals indicate that the specific interfacial water structure on calcite is decisive for rationalizing the self-assembly of Benzopurpurine 4B in this system.

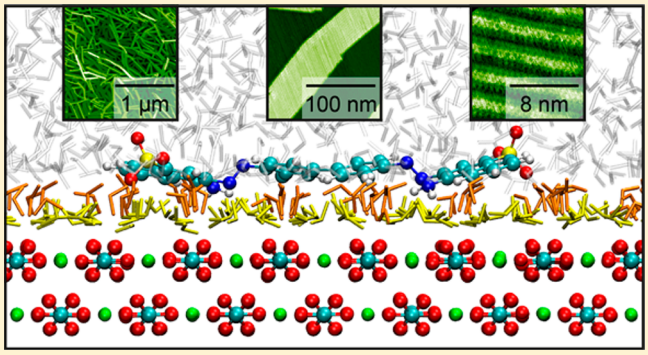

INTRODUCTION

Self-assembly is a powerful tool for creating functional molecular structures at surfaces.[1,2] Thus far, however, most reported examples are limited to systems kept in ultrahigh vacuum (UHV)[3−8] or at ambient conditions.[9,10] At solid–liquid interfaces, despite being of tremendous importance both in nature and in technology,[11−14] only limited progress has been made in terms of rationally controlling molecular self-assembly by an informed choice of suitable molecules and/or solvent.[15−19] The formation of well-ordered structures on solid surfaces is steered by the subtle balance of molecule–surface and molecule–molecule interactions.[20] At solid–liquid interfaces, the complexity of the situation is increased because additional molecule–solvent, surface–solvent, and solvent–solvent interactions play a decisive role in determining the adsorption configuration. This complexity severely hampers the rational control of self-assembly at the mineral–water interface. For example, for many molecules studied at the mineral–water interface, it even remains impossible to predict whether or not an ordered structure will form.

In-situ dynamic atomic force microscopy (AFM) has been shown to provide atomic and molecular resolution information for mineral surfaces,[21,22] molecular[23−28] and hydration structures,[29−35] as well as the possibility of chemical identification at the solid–liquid interface.[36] Nevertheless, a comprehensive molecular understanding of adsorption and self-assembly processes is still missing, and computer modeling has been often used to further our knowledge.

For calcite, the most stable polymorph of calcium carbonate ($CaCO_3$) at ambient conditions and its natural cleavage plane (10.4) (Figure 1a) extensive simulation studies have helped yield a molecular-scale picture of the interfacial structure, which agrees remarkably well with experiment.[37−40] Computational work has also been used to understand the interaction of organic molecules with calcium carbonate. Benzopurpurine 4B (BPP, Figure 1b) is a commonly used textile dye[41,42] and structurally closely related to Congo Red, which has previously been studied with *in-situ* dynamic AFM on the calcite (10.4) cleavage plane.[27] Congo Red has been shown to drastically restructure the calcite (10.4) surface, indicative of a strong molecule–surface interaction perhaps mediated through the negatively charged sulfonate (SO_3^-) groups. Therefore, a strong molecule–calcite interaction might be expected for BPP as well. In the present study, we use a combination of *in-situ* AFM and computer simulation to examine whether this is indeed the case.

Received: October 4, 2017
Published: October 9, 2017

DOI: 10.1021/acs.jpcc.7b09825
J. Phys. Chem. C 2017, 121, 24144−24151

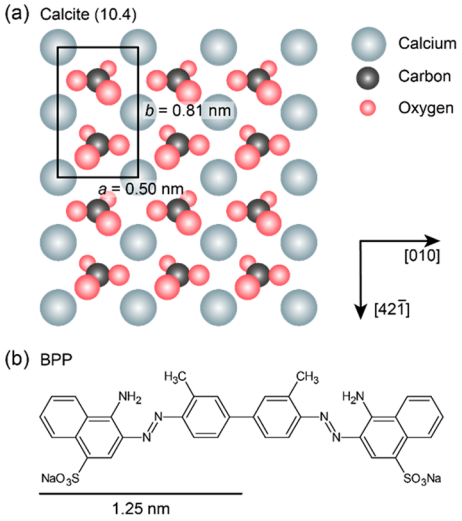

Figure 1. (a) Structure of the calcite (10.4) surface. (b) Chemical structure of Benzopurpurine 4B (BPP). Scale bar below (b) applies to both parts of the figure.

MATERIALS AND METHODS

Solution Preparation. Benzopurpurine 4B (BPP) was purchased from TCI Deutschland GmbH as a disodium salt and used without further purification. Pure water (18.2 MΩ·cm) was produced using a purification setup from Merck Millipore. Sodium hydroxide (NaOH, 0.1 and 1 M) and hydrochloric acid (HCl, 0.1 and 1 M) standard solutions were used to adjust the pH of the solutions and purchased from Carl Roth GmbH & Co. KG. All pH measurements were conducted using a Schott laboratory pH meter (CG 842) equipped with a BlueLine pH electrode (Schott Instruments, 18 pH). The pH electrode was calibrated weekly, utilizing buffer standard solutions with pH values of 4 and 7 (HANNA instruments, types Hi6004 and Hi6007).

***In-Situ* Dynamic Atomic Force Microscopy Imaging.** Calcite crystals were purchased from Korth Kristalle GmbH, freshly cleaved, and cleaned with a nitrogen flow prior to each experiment. All images shown here were taken at a constant temperature of 28 °C using a modified commercial atomic force microscope (AFM) from Bruker Corp. (MultiMode V with Nanoscope V controller) operated in the frequency modulation (FM) mode. The FM-AFM setup has been optimized for high-resolution imaging in a liquid environment.[43,44] All *in-situ* FM-AFM experiments were conducted with a liquid cell from Bruker Nano Surfaces Division. We used gold-coated and p-doped silicon cantilevers (PPP-NCHAuD, Nanosensors and Tap300GD-G, BudgetSensors) with a typical eigenfrequency of 100−150 kHz in liquids and a spring constant of ∼40 N/m. The oscillation amplitude of the cantilever was kept constant at 1 nm for all measurements. In all AFM images shown here, the slow and fast scan direction and the measured channel are displayed in the schematics in the upper right corner.

Measurement Conditions. With respect to calcium carbonate solubility, all *in-situ* AFM measurements were conducted in an undersaturated solution, only consisting of pure water, solute BPP, and, depending on the starting conditions, hydrochloric acid or sodium hydroxide. An immersed calcite crystal in an undersaturated solution dissolves at all times, independent of the pH, until dynamic carbonate equilibrium is reached. Calcite dissolution releases calcium (Ca^{2+}) and carbonate (CO_3^{2-}) ions into the surrounding solution, the latter causing the pH to converge to a value of around 8.3,[45] which corresponds to the carbonate equilibrium. Because the pH is not measurable during the *in-situ* AFM experiment, we note that stated pH values correspond to the initial pH of the solution, which was adjusted and measured prior to injection in the liquid cell. As the liquid cell used is open to air, evaporation undoubtedly takes places at all times during the *in-situ* AFM experiment, slowly increasing the concentration of all components in the solution. Therefore, the indicated BPP concentrations also refer to the initial concentrations as prepared.

Molecular Dynamics Simulation. Molecular dynamics (MD) simulations of BPP in water with and without a calcite slab were performed using the LAMMPS code[46] augmented with the PLUMED2.2 plugin[47] for calculation of the pairing and adsorption free energies. All simulations were performed at constant volume (NVT) after an initial equilibration of the cell volume at 1 atm. The equations of motions were integrated using the velocity-Verlet algorithm with a 1 fs time step, and the temperature was kept at 300 K with a chain of 5 Nosé−Hoover thermostats and a relaxation time of 0.1 ps. The GAFF1.7 force field[48] was used to describe the BPP−BPP, BPP−water, and BPP−calcite/gypsum interactions as well as the intramolecular component for BPP; the calcite and sodium/calcite−water interactions come from previous works,[39,49−51] while the gypsum water interactions were taken from our recent work.[52] It is important to note here that the calcite−water and gypsum−water interactions used in this work have been carefully parametrized and tested against thermodynamic experimental data that include the hydration free energy of the ions, the solubility of calcite, the Ca−CO_3 ion pair association constant, as well as the water structure above the calcite surface that compares well with X-ray reflectivity data. Moreover, the SPC/Fw water model[53] used in this work gives an accurate representation of the liquid phase over a wide range of temperatures. Properties, such as the water solvation free energy, dielectric constant, and structure, are found to be in good agreement with experiment for this water model.[49] On the other hand, the interactions involving BPP are much harder to benchmark due to the lack of experimental data to compare against; quantities such as the solvation free energy of BPP or the BPP−calcium pairing free energy are indeed unknown. Due to the complexity of the molecule, it is currently too expensive to run *ab initio* calculations in bulk water for a sufficiently long time to obtain benchmark data against which to calibrate the force field. Although the precise quantitative values of the association and adsorption free energies obtained from the simulations need to be treated with appropriate caution, we believe the simulations can qualitatively reproduce and explain the experimental observations.

The free energy calculations were performed using the multiple walkers well-tempered metadynamics technique,[54−56] and a bias factor of 12 was chosen to ensure convergence of the calculations. The initial Gaussian height was set to k_BT and their width to 0.2 Å. The pairing free energy between two BPP molecules was calculated by inserting two dye molecules and 4 Na^+ ions in a ∼100 Å box of water with 3D periodic boundary conditions (PBC). Because of the size of BPP the pairing mechanism could be quite complex and the reaction coordinate is not immediately evident, as for two monatomic or small ions. We therefore repeated the calculations using two different collective variables (CV): the mean distance between all atoms

DOI: 10.1021/acs.jpcc.7b09825
J. Phys. Chem. C 2017, 121, 24144−24151

in the two BPP molecules and the distance between their centers of mass, as implemented in PLUMED2.2. The adsorption free energies of BPP on the calcite (10.4) and gypsum (020) surfaces were computed using a 3D periodic cell containing a 12 and 8 layer thick slab, respectively. A 6 × 10 (10 × 10) surface supercell of calcite (gypsum) was created and separated from its periodic image by a space of approximately 40 Å (60 Å), which was then filled with water at the density of the bulk liquid. One BPP molecule and two Na^+ counterions were also inserted in the box. As the CV, we used the z component of the distance between the center of mass of BPP and a Ca^{2+} ion in the middle of the mineral slab.

In the case of calcite, we also considered the adsorption of a second BPP molecule on the mineral surface to form an adsorbed dimer, which could be regarded as the first nucleus of a BPP island. Because of the many different available pathways for this process this is a very computationally challenging task and some simplifications of the problem are necessary. In order to estimate the adsorption free energy, we restrained one BPP to stay in the adsorbed state by using a harmonic potential acting on the z component of the distance between the BPP center of mass and one calcium atom deep in the calcite slab. In order to minimize the effect of the restraint we used a spring constant of 0.4 eV/Å^2, which follows the adsorption free energy profile for one molecule. As a collective variable for the metadynamics calculations we decided to use the z component of the distance between the centers of mass of the two BPP molecules, and to limit the configurational space to be explored we placed harmonic "walls" at 20 Å. The bias factor was also reduced to 8 to accelerate the convergence.

Unbiased MD simulations of a stack of 8 BPP molecules on the (10.4) surface of calcite have been performed in the NVT ensemble to assess the stability of the stack and assess whether the oscillations in the *in-situ* AFM measurements are compatible with this structure. The stack has been built by replicating one of the configurations of the dimers 4 times along an axis normal to the BPP aromatic system. After the stack has been inserted above the calcite surface the pressure was equilibrated by varying the z axis in a 5 ns NPT run and the system was then further run for 15 ns in the NVT ensemble.

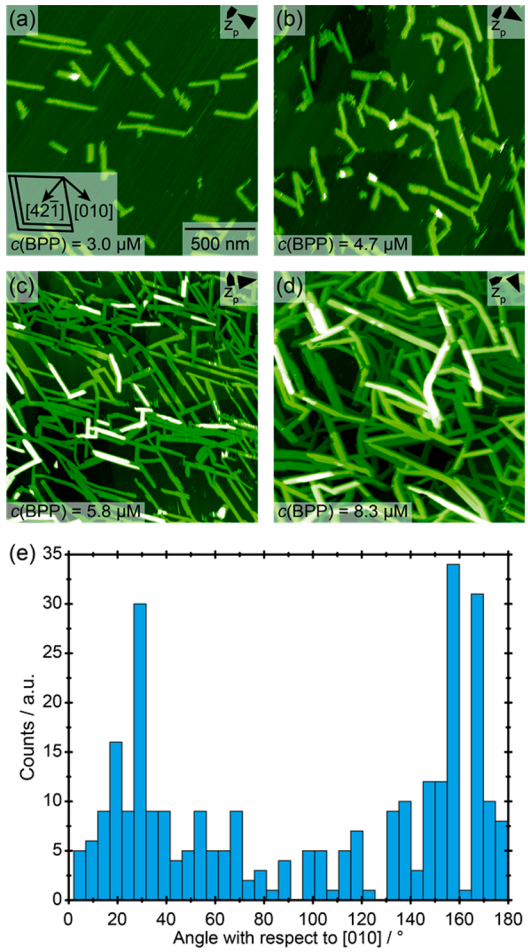

Figure 2. Representative AFM images illustrating the elongated BPP islands on calcite (10.4) as a function of BPP concentration. Calcite (10.4) surface in the presence of 3.0, 4.7, 5.8, and 8.3 μM BPP, from left to right, at a fixed solution pH of 3.5. Scale bar in a applies to all images in this series. Variation of the pH in a range from pH 3.5 to 11 did not reveal any influence of the pH on the island shape reported here. (e) Angle histogram illustrating the orientation of the islands with respect to the underlying calcite lattice.

RESULTS AND DISCUSSION

Here, *in-situ* dynamic AFM shows the formation of oblong islands (Figure 2) that exhibit a rather uniform width distribution between 40 and 70 nm. Increasing the concentration allows for control of the number of molecules at the interface. While only a few monolayer islands are observed at a low concentration of 3.0 μM (Figure 2a), multilayer islands are seen at a concentration of 8.3 μM (Figure 2d). Interestingly, the islands exhibit various orientations with respect to the underlying substrate lattice. In particular, the high-symmetry directions [010], [0$\bar{1}$0], [42$\bar{1}$], and [$\bar{4}$2$\bar{1}$] as well as the etch pits directions [$\bar{4}$4$\bar{1}$], [$\bar{4}$41], [48$\bar{1}$], and [$\bar{4}$8$\bar{1}$]—corresponding to the angles 0°, 90°, 39°, and 129°—do not appear to be favored. To quantify the latter observation, we present an angle histogram in Figure 2e, illustrating that a broad angle distribution can be found with no clear tendency for a certain island orientation.

At low concentration, the profile line measured across one 70 nm wide BPP island (Figure 3a) shows an apparent height of 2.2 nm (Figure 3b), while at high concentrations the formation of multilayer islands with heights of up to 10 nm were observed. It should be stressed that AFM—similar to other scanning probe microscopy techniques—does not provide true topography information. Therefore, while lateral periodicities can be provided with high accuracy, vertical heights have to be considered with care, which is why we refer to an apparent height. A high-resolution image of one of the BPP islands reveals ordered molecular stripes within the island (Figure 3c) with a stripe-to-stripe distance of approximately 3.5 nm (Figure 3d). Additionally, a periodicity within one stripe of approximately 0.8 nm could also be measured (Figure 3e).

In order to rationalize the experimental observations we used computer simulations to estimate the strength of BPP−BPP interactions, as well as the adsorption free energy of BPP on the calcite (10.4) surface. It is well known that organic dyes in aqueous solution tend to form stacks at high concentration,[42,57−60] and BPP has been reported to form aggregates as long as several micrometers.[42] As per our previous work on the Sunset Yellow dye,[61] we calculated the free energy to separate two BPP molecules in water using metadynamics simulations.[54] The computed binding free energy is −31.5 or −35.5 kJ/mol (Figure S1), depending on the choice of collective variable, which is similar to the value for Sunset Yellow (−28 kJ/mol[61])

DOI: 10.1021/acs.jpcc.7b09825
J. Phys. Chem. C 2017, 121, 24144−24151

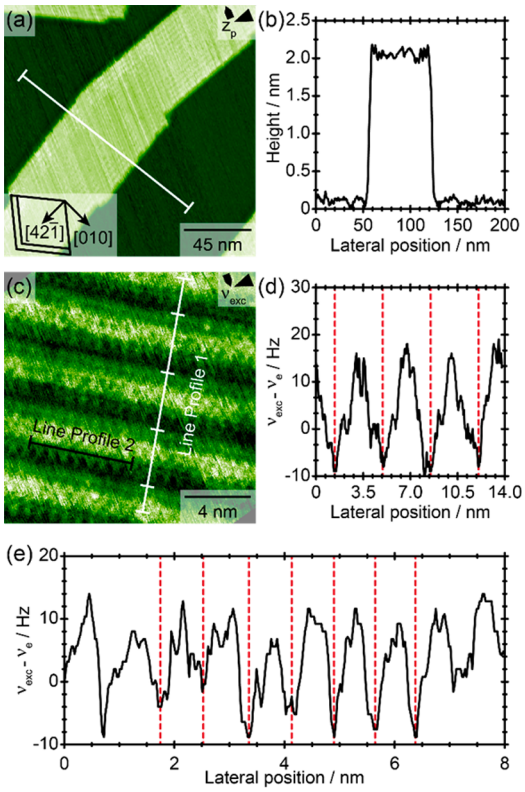

Figure 3. Molecular adsorption of BPP on the calcite (10.4) surface. (a) AFM image showing a BPP island on calcite (10.4) at a solution pH of 7.7 (c(BPP) = 72 μM). (b) Line profile taken at the indicated position in a, revealing an island width of 70 nm and an apparent island height of approximately 2.2 nm. (c) Drift-corrected, high-resolution frequency shift image of the molecular structure of a BPP island on the same sample. (d) Line profile 1 taken at the indicated position in c, revealing a stripe-to-stripe distance of approximately 3.5 nm. (e) Line profile 2 taken at the indicated position in c, revealing a periodicity of approximately 0.8 nm within a molecular stripe.

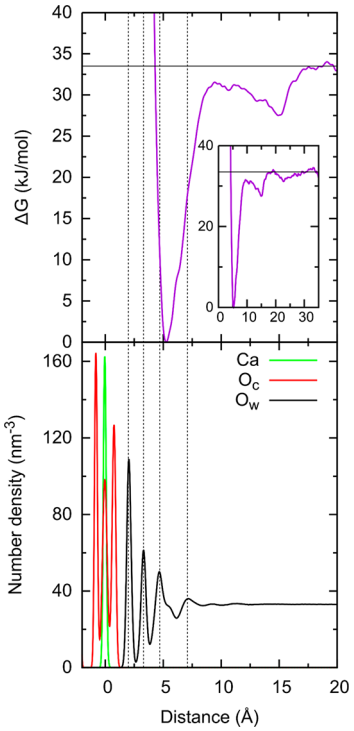

Figure 4. Free energy of a single BPP molecule adsorbed onto calcite (10.4) as a function of distance from the surface relative to the most stable adsorption site (top) and density profiles (bottom) for calcium (green) carbonate oxygen (red) and water oxygen (black). Position of the calcite surface, defined as the average position of the top Ca layer, is set to zero. Dashed vertical lines mark the positions of the four main peaks in the water density profile, while solid horizontal black line at 33.5 kJ/mol indicates the estimated adsorption free energy of BPP on the calcite (10.4) surface.

and an experimental estimate (~−26 kJ/mol[42]). For both BPP and Sunset Yellow, force field simulations predict a binding between the dyes that is up to 10 kJ/mol stronger than the experimental estimates. Although there might be some fundamental differences between the calculated free energy and the experimental estimates, this discrepancy is most likely to be due to a systematic error in the force field hydration free energies. Analogously to Sunset Yellow, the molecules in a BPP dimer prefer a parallel arrangement (Figure S2) that maximizes $\pi-\pi$ stacking and minimizes the amount of "surface" exposed to water. Due to this large exothermic binding free energy, the formation of aggregates (stacks) in solution is thermodynamically favorable, despite the negative charge on the molecules, and is responsible for the formation of liquid crystals at high concentrations.[42,57−60] However, the BPP concentrations used in the present work (1.7−110 μM) are much lower than those required to form liquid crystals and simple models[61,62] that predict the average number of molecules in aggregates indicate that BPP is largely isolated in solution. It is therefore safe to assume that the adsorption of BPP on calcite is likely to proceed one molecule at a time, rather than via preassembled stacks.

Our calculations of the adsorption of BPP on the basal plane of calcite predict the adsorption free energy is approximately −33.5 kJ/mol (Figure 4) and shows that the most stable adsorbed state has the BPP lying flat relative to the surface (Figure 5), while the shallow minimum at 15 Å above the surface corresponds to configurations where BPP is perpendicular to the surface plane (Figure S3).

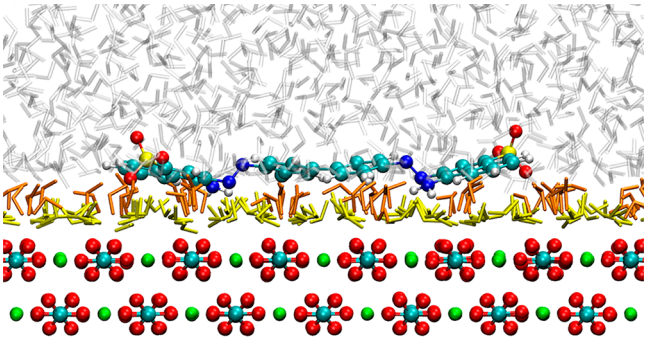

Figure 5. Representative atomic configuration corresponding to the free energy minimum in Figure 4 is shown with calcium, carbon, oxygen, sulfur, nitrogen, and hydrogen colored green, light blue, red, yellow, dark blue, and white, respectively. Water molecules of the first calcite hydration layer are shown in yellow, those in the second hydration layer are shown in orange, and those in subsequent weaker layers and bulk water are shown as transparent gray molecules. Positions of the atoms of the mineral were averaged over 5 ps to reduce noise, while positions of the water and BPP atoms are from one single frame.

DOI: 10.1021/acs.jpcc.7b09825
J. Phys. Chem. C 2017, 121, 24144−24151

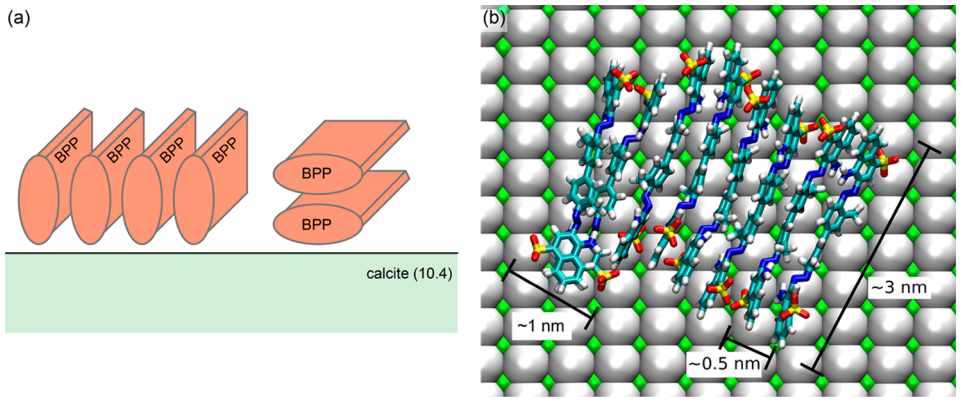

Figure 6. (a) Schematic representation of the possible arrangements of the BPP molecules in the adsorbed islands showing the perpendicular (left) and parallel (right) configurations. (b) Sample atomic configuration of a stack of eight BPP molecules on calcite (10.4) after ∼15 ns of MD equilibration. For clarity, the water molecules are removed and the carbonate ions of the calcite top layer are represented as large white spheres. Scale bars shown on the plot are approximate and determined from the atomic trajectories.

The somewhat surprising finding is that in both adsorbed states BPP is never in contact with the calcite surface, but instead lays on top of the second ordered water layer (Figure 5). The above observation can be rationalized by considering that BPP has large hydrophobic sections and therefore tries to minimize its interaction with bulk water (Figure S4), an effect that, together with $\pi-\pi$ interaction, is also responsible for the formation of long stacks of organic dyes in aqueous solution. When BPP approaches the calcite surface there are already two well-organized water layers in which the water molecules are strongly coordinated to the calcium ions (first layer) or hydrogen bonded to carbonate (second layer).[37,39,63] The orientation of the water molecules above the calcite surface is therefore strongly dictated by the presence of the mineral, and the hydrogen bonds of these two layers with bulk water are weakened. Consequently, the adsorption of BPP on the second water layer has a smaller energy penalty than remaining in bulk water, where water molecules on both sides of BPP would incur a penalty for reorganizing their hydrogen-bonding network. Moreover, removing the strongly bound water molecules from the first two layers to allow for direct binding of BPP to the calcite surface is also highly unfavorable (Figure 4). By borrowing a terminology commonly used in organic chemistry we can say that the adsorption of BPP on calcite is driven by a "hydrophobic effect" rather than—as might be initially assumed—by electrostatic interactions with the mineral surface. Small regions of BPP, like the sulfonate ($-SO_3^-$) groups, the amino ($-NH_2$) groups, or the diazo (—N═N—) bridges, can still interact electrostatically with the ionic surface of calcite, but because of the relatively long range (>5 Å) and the screening from the water layers, the forces are generally weak. This is consistent with the experimental observation that there is no preferred orientation for the adsorbed BPP molecules on the surface.

The adsorption free energy for a second BPP molecule to form a dimer on the calcite surface was also estimated by metadynamics calculations and found to be on the order of −47.7 kJ/mol (Figure S5). This is larger than the pairing free energy obtained in bulk water, but because of the complexity of the calculations, we do not necessarily regard this difference as being significant since there may be convergence issues or artifacts due to the restraint that holds one BPP over the surface. Nevertheless, this confirms that the formation of BPP dimers on the surface of calcite is thermodynamically favorable. Two possible dimer arrangements can be envisioned, one with the dimers standing sideways on the surface and one with the dimers laying parallel to the surface (see Figure 6a). Analysis of the atomic trajectories showed that one of the stable configurations for the adsorbed dimer has both molecules standing sideways on the surface, which was then used to build a small island and assess its stability on the calcite surface. The small BPP island remained stable for the whole simulation (∼20 ns), though after ∼10 ns the two end molecules on one side turned to form a dimer that is aligned almost parallel to the surface (Figure 6b), i.e., the turned dimer represents the other dimer configuration shown in the schematic in Figure 6a.

It is worth noting that during the above simulations the BPP stack never came into direct contact with the calcite surface but remained doubly solvent separated, as in the case of the adsorption of a single molecule or the dimer, and that the island slowly rotated during the MD run. These findings provide evidence for the fact that there is only a weak direct interaction between the calcite surface and BPP that might lead to a preferred orientation. Regardless of the dimer orientation, the width of the simulated BPP stack (∼3 nm) indicates that the experimentally observed stripes are composed of such BPP stacks, which arrange with a stripe-to-stripe distance of ∼3.5 nm (Figure 3d). The separation between the molecules stacked perpendicularly to the surface (0.3−0.5 nm) is consistent with the typical $\pi-\pi$ stacking distance, which is one-half the periodicity observed experimentally (approximately 0.8 nm, Figure 3e). This factor of 2 could be due to specific AFM imaging conditions. For example, even for bare calcite it is known that certain tips image two surface features as a single one (so-called row pairing).[64] Thus, it is possible that we image pairs of molecules aligned sideways. Another option is that the islands were instead formed by flat-laying BPP dimers aligned next to each other. Then the width of the dimers would be approximately 1 nm, which would then require the dimers to arrange in an overlapping manner to agree with the experimentally observed periodicity of 0.8 nm (Figure 3e). Both arrangements shown in Figure 4a seem to be plausible, and it is difficult to obtain quantitative information regarding their relative stability. The height of a BPP dimer relative to the surface is very similar to that of a BPP molecule standing sideways on the surface (from the MD trajectories, the highest atoms sit between 1 and 2 nm above the surface, defined as the z position of the calcium ions), and therefore, the apparent

DOI: 10.1021/acs.jpcc.7b09825
J. Phys. Chem. C 2017, 121, 24144−24151

height observed in the AFM measurements for both these structures would be very similar. Because the apparent height in the AFM images would also depend on the structure of the water layers above the island, it is difficult to definitively rule out one arrangement or the other. Moreover, if we consider that a macroscopic BPP island carries a significant negative charge, it is likely that Na^+ ions would be intercalated between the molecules and within the stripes, increasing both the intermolecular separation and the stack width measured from the MD simulations, an effect not considered in this work.

The above discussion highlights the impact of the interfacial hydration structure on the self-assembly of BPP on calcite (10.4). To further verify this interpretation we performed *in-situ* AFM measurements on three further substrates, namely, muscovite mica (0001), gypsum ($CaSO_4 \cdot 2H_2O$) (020), and calcium fluoride (CaF_2) (111) surfaces. As can be seen in Figure S6, for none of these surfaces could we observe any adsorption of molecular islands when using a BPP concentration of 18−83 μM at a pH of 3.5. These results strengthen our hypothesis that the observed adsorption of BPP on calcite is strongly related to the presence of the first two well-ordered water layers on this mineral's surface (Figures 4 and 5). In particular, we argue that the key features that favor the adsorption of hydrophobic species on the hydrated calcite surface are the presence of strong hydrogen bonds between the water molecules in the second water layer and the mineral surface.

In the case of mica there is no clear separation between the second and the third water layer,[65,66] and the presence of cations in the Stern layer, which are necessary for the local charge neutrality of the system, is probably responsible for the disruption of the hydrogen-bond network and of any lateral ordering of the hydration water. In the case of CaF_2, computer simulations of the water structure above the (111) surface[67] show that there are three well-defined water layers above the surface. Similar to calcite, the water molecules in the first hydration layer are strongly localized above the calcium ions and lay mostly flat above the surface. However, because fluoride (F^-) is not a good hydrogen-bond acceptor, the water molecules in the second hydration layer are oriented differently to those on calcite and form hydrogen bonds with the molecules in the third hydration layer.[67] This observation is consistent with the third water layer being further away from the mineral surface for CaF_2 than for calcite.

More interesting is the case of gypsum where the sulfate groups at the surface could form hydrogen bonds with water, and it was, therefore, expected to behave similarly to calcite. The 1D water density profiles above the two mineral surfaces is, however, markedly different (Figure S7), and in agreement with the experimental results, metadynamics simulations predict that BPP should not adsorb on the (020) gypsum surface (Figure S8). Although three water layers can be clearly identified also above the (020) gypsum surface, these layers are significantly closer to the mineral surface (defined as the position of the topmost calcium layer) compared to calcite, and the second and third layers almost overlap. By analyzing the position and orientation of the water molecules above the gypsum (020) surface (Figures S7 and S9) it is evident that the first hydration layer could be considered as a continuation of the mineral lattice and that, similarly to calcite, the molecules in the second layer form strong hydrogen bonds with the sulfate ions at the surface. However, a detailed analysis of the geometry of the hydrogen bonds between the water and the mineral surfaces as a function of the distance from the surface reveals some interesting differences between the two minerals (Figure S10). A typical hydrogen bond in bulk water is characterized by an oxygen−oxygen distance of approximately 2.7 Å and an O−H−O bond of approximately 165° (Figure S11), and any deviations from this typical configuration would result in a weaker hydrogen bond. It is, therefore, immediately evident that the strongest hydrogen bonds between water and the mineral surface are formed by the molecules in the second hydration layer above the calcite (10.4) surface and those in the first hydration layer above the gypsum (020) surface, while there are virtually no hydrogen bonds between calcite and its first hydration layer and between gypsum and its second hydration layer. The third hydration layer also forms very weak hydrogen bonds with both minerals due to its larger distance from the surfaces. This observation supports our hypothesis that the second water layer above calcite has a strong lateral ordering due to the interaction with the mineral, and it is, therefore, an optimal place for BPP due to the lower entropic cost associated with locating a hydrophobic adsorbent on top of the second layer rather than in the bulk solution. On the other hand, the second hydration layer above the gypsum (020) surface forms very weak hydrogen bonds with the mineral; hence, it has a smaller lateral ordering, and it can be viewed as more "bulk-like". Therefore, there is no entropic gain for BPP to leave the bulk solution and adsorb on gypsum. From this comparison we can conclude that the specific hydration layer structure is critical for the adsorption of organic molecules at the interface. Interestingly, even seemingly similar surfaces such as calcite (10.4) and gypsum (020) can greatly vary in their interaction with hydrophobic molecules due to details of their hydration structure.

CONCLUSIONS

Using *in-situ* high-resolution dynamic AFM and MD calculations we studied the adsorption of BPP at the calcite (10.4)−water interface. BPP forms well-ordered molecular islands that appear not to be commensurate with respect to the underlying substrate lattice. The islands exhibit a characteristic inner structure with lateral periodicities of about 3.5 and 0.8 nm. From MD simulations and free energy calculations we find that BPP does not bind to the calcite (10.4) surface directly but instead adopts a position above the second hydration layer. This unexpected adsorption position can be understood by the fact that the water structure is least disturbed by the molecule when positioned in the most hydrophobic region, which is atop the second hydration layer. This finding rationalizes why the experimentally observed islands are not commensurate with the underlying calcite lattice, which in turn supports the finding of the simulations. We corroborate this finding by comparing the results obtained on calcite (10.4) with other mineral surfaces that exhibit different interfacial hydration structures and show that the formation of the island-like structures of BPP seems to be highly selective for the calcite (10.4) surface, despite the lack of direct interaction, because of the unique structure of its mineral−water interface.

ASSOCIATED CONTENT

Supporting Information

The Supporting Information is available free of charge on the ACS Publications website at DOI: 10.1021/acs.jpcc.7b09825.

DOI: 10.1021/acs.jpcc.7b09825
J. Phys. Chem. C 2017, 121, 24144−24151

Additional *in-situ* AFM and computer simulation data (PDF)

AUTHOR INFORMATION

Corresponding Authors

*E-mail: p.raiteri@curtin.edu.au.

*E-mail: kuehnle@uni-mainz.de.

ORCID

Martin Nalbach: 0000-0003-0045-7548

Paolo Raiteri: 0000-0003-0692-0505

Angelika Kühnle: 0000-0003-1214-1006

Author Contributions

The manuscript was written through contributions of all authors. All authors have given approval to the final version of the manuscript. The authors declare no competing financial interests.

Notes

The authors declare no competing financial interest.

ACKNOWLEDGMENTS

A.K. acknowledges financial support by the German Research Foundation through project KU1980/7-1. P.R. and J.D.G. thank the Australian Research Council for financial support through the Discovery Programme (FT130100463, DP160100677) and the Pawsey Supercomputing Centre and National Computational Infrastructure for the provision of computer time. P.R. would also like to thank Dr. B. Reischl for sharing the atomic trajectories for the water structure on the CaF_2 (111) surface.

ABBREVIATIONS

BPP	benzopurpurine 4B
FM-AFM	frequency modulation atomic force microscopy
MD	molecular dynamics

REFERENCES

(1) Whitesides, G. M.; Mathias, J. P.; Seto, C. T. Molecular Self-Assembly and Nanochemistry: A Chemical Strategy for the Synthesis of Nanostructures. *Science* **1991**, *254*, 1312−19.

(2) Barth, J. V. Molecular Architectonic on Metal Surfaces. *Annu. Rev. Phys. Chem.* **2007**, *58*, 375−407.

(3) Rosei, F.; Schunack, M.; Jiang, P.; Gourdon, A.; Lægsgaard, E.; Stensgaard, I.; Joachim, C.; Besenbacher, F. Organic Molecules Acting as Templates on Metal Surfaces. *Science* **2002**, *296*, 328−331.

(4) Barlow, S. M.; Raval, R. Complex Organic Molecules at Metal Surfaces: Bonding, Organisation and Chirality. *Surf. Sci. Rep.* **2003**, *50*, 201−341.

(5) Barth, J. V.; Costantini, G.; Kern, K. Engineering Atomic and Molecular Nanostructures at Surfaces. *Nature* **2005**, *437*, 671−679.

(6) Glatzel, T.; Zimmerli, L.; Koch, S.; Kawai, S.; Meyer, E. Molecular Assemblies Grown between Metallic Contacts on Insulating Surfaces. *Appl. Phys. Lett.* **2009**, *94*, 063303.

(7) Hauke, C. M.; Bechstein, R.; Kittelmann, M.; Storz, C.; Kilbinger, A. F.; Rahe, P.; Kühnle, A. Controlling Molecular Self-Assembly on an Insulating Surface by Rationally Designing an Efficient Anchor Functionality That Maintains Structural Flexibility. *ACS Nano* **2013**, *7*, 5491−5498.

(8) Rahe, P.; Kittelmann, M.; Neff, J. L.; Nimmrich, M.; Reichling, M.; Maass, P.; Kühnle, A. Tuning Molecular Self-Assembly on Bulk Insulator Surfaces by Anchoring of the Organic Building Blocks. *Adv. Mater.* **2013**, *25*, 3948−56.

(9) Love, J. C.; Estroff, L. A.; Kriebel, J. K.; Nuzzo, R. G.; Whitesides, G. M. Self-Assembled Monolayers of Thiolates on Metals as a Form of Nanotechnology. *Chem. Rev.* **2005**, *105*, 1103−1170.

(10) McGuiness, C. L.; Shaporenko, A.; Mars, C. K.; Uppili, S.; Zharnikov, M.; Allara, D. L. Molecular Self-Assembly at Bare Semiconductor Surfaces: Preparation and Characterization of Highly Organized Octadecanethiolate Monolayers on Gaas(001). *J. Am. Chem. Soc.* **2006**, *128*, 5231−5243.

(11) Brown, G. E., Jr. Surface Science - How Minerals React with Water. *Science* **2001**, *294*, 67−69.

(12) Brown, G. E., Jr.; Calas, G. Mineral-Aqueous Solution Interfaces and Their Impact on the Environment. *Geochemical Perspectives* **2012**, 483−742.

(13) Putnis, C. V.; Ruiz-Agudo, E. The Mineral-Water Interface: Where Minerals React with the Environment. *Elements* **2013**, *9*, 177−182.

(14) Putnis, A. Why Mineral Interfaces Matter. *Science* **2014**, *343*, 1441−1442.

(15) Lackinger, M.; Griessl, S.; Heckl, W. A.; Hietschold, M.; Flynn, G. W. Self-Assembly of Trimesic Acid at the Liquid-Solid Interface - a Study of Solvent-Induced Polymorphism. *Langmuir* **2005**, *21*, 4984−4988.

(16) Destoop, I.; Ghijsens, E.; Katayama, K.; Tahara, K.; Mali, K. S.; Tobe, Y.; De Feyter, S. Solvent-Induced Homochirality in Surface-Confined Low-Density Nanoporous Molecular Networks. *J. Am. Chem. Soc.* **2012**, *134*, 19568−19571.

(17) Sirtl, T.; Song, W.; Eder, G.; Neogi, S.; Schmittel, M.; Heckl, W. M.; Lackinger, M. Solvent-Dependent Stabilization of Metastable Monolayer Polymorphs at the Liquid−Solid Interface. *ACS Nano* **2013**, *7*, 6711−6718.

(18) Tahara, K.; Kaneko, K.; Katayama, K.; Itano, S.; Nguyen, C. H.; Amorim, D. D. D.; De Feyter, S.; Tobe, Y. Formation of Multicomponent Star Structures at the Liquid/Solid Interface. *Langmuir* **2015**, *31*, 7032−7040.

(19) Della Pia, A.; Luo, D.; Blackwell, R.; Costantini, G.; Martsinovich, N., Molecular Self-Assembly of Substituted Terephthalic Acids at the Liquid/Solid Interface. *Faraday Discuss.* **2017**.10.1039/C7FD00112F

(20) Otero, R.; Gallego, J. M.; de Parga, A. L.; Martin, N.; Miranda, R. Molecular Self-Assembly at Solid Surfaces. *Adv. Mater.* **2011**, *23*, 5148−76.

(21) Fukuma, T.; Kobayashi, K.; Matsushige, K.; Yamada, H. True Atomic Resolution in Liquid by Frequency-Modulation Atomic Force Microscopy. *Appl. Phys. Lett.* **2005**, *87*, 034101.

(22) Rode, S.; Oyabu, N.; Kobayashi, K.; Yamada, H.; Kühnle, A. True Atomic-Resolution Imaging of (1014) Calcite in Aqueous Solution by Frequency Modulation Atomic Force Microscopy. *Langmuir* **2009**, *25*, 2850−2853.

(23) Fukuma, T.; Kobayashi, K.; Matsushige, K.; Yamada, H. True Molecular Resolution in Liquid by Frequency-Modulation Atomic Force Microscopy. *Appl. Phys. Lett.* **2005**, *86*, 193108.

(24) Hiasa, T.; Kimura, K.; Onishi, H. Cross-Sectional Structure of Liquid 1-Decanol over Graphite. *J. Phys. Chem. C* **2012**, *116*, 26475−26479.

(25) Schreiber, M.; Eckardt, M.; Klassen, S.; Adam, H.; Nalbach, M.; Greifenstein, L.; Kling, F.; Kittelmann, M.; Bechstein, R.; Kühnle, A. How Deprotonation Changes Molecular Self-Assembly - an Afm Study in Liquid Environment. *Soft Matter* **2013**, *9*, 7145−7149.

(26) De Yoreo, J. J.; Chung, S.; Friddle, R. W. Situ Atomic Force Microscopy as a Tool for Investigating Interactions and Assembly Dynamics in Biomolecular and Biomineral Systems. *Adv. Funct. Mater.* **2013**, *23*, 2525−2538.

(27) Momper, R.; Nalbach, M.; Lichtenstein, K.; Bechstein, R.; Kühnle, A. Stabilization of Polar Step Edges on Calcite (10.4) by the Adsorption of Congo Red. *Langmuir* **2015**, *31*, 7283−7287.

(28) Nalbach, M.; Klassen, S.; Bechstein, R.; Kühnle, A. Molecular Self-Assembly Versus Surface Restructuring During Calcite Dissolution. *Langmuir* **2016**, *32*, 9975−9981.

(29) Fukuma, T.; Ueda, Y.; Yoshioka, S.; Asakawa, H. Atomic-Scale Distribution of Water Molecules at the Mica-Water Interface Visualized by Three-Dimensional Scanning Force Microscopy. *Phys. Rev. Lett.* **2010**, *104*, 016101.

DOI: 10.1021/acs.jpcc.7b09825
J. Phys. Chem. C 2017, 121, 24144−24151

(30) Suzuki, K.; Oyabu, N.; Kobayashi, K.; Matsushige, K.; Yamada, H. Atomic-Resolution Imaging of Graphite−Water Interface by Frequency Modulation Atomic Force Microscopy. *Appl. Phys. Express* **2011**, *4*, 125102.
(31) Imada, H.; Kimura, K.; Onishi, H. Water and 2-Propanol Structured on Calcite (104) Probed by Frequency-Modulation Atomic Force Microscopy. *Langmuir* **2013**, *29*, 10744−10751.
(32) Labuda, A.; Kobayashi, K.; Suzuki, K.; Yamada, H.; Grütter, P. Monotonic Damping in Nanoscopic Hydration Experiments. *Phys. Rev. Lett.* **2013**, *110*, 066102.
(33) Marutschke, C.; Walters, D.; Cleveland, J.; Hermes, I.; Bechstein, R.; Kühnle, A. Three-Dimensional Hydration Layer Mapping on the (10.4) Surface of Calcite Using Amplitude Modulation Atomic Force Microscopy. *Nanotechnology* **2014**, *25*, 335703.
(34) Fukuma, T.; Reischl, B.; Kobayashi, N.; Spijker, P.; Canova, F. F.; Miyazawa, K.; Foster, A. S. Mechanism of Atomic Force Microscopy Imaging of Three-Dimensional Hydration Structures at a Solid-Liquid Interface. *Phys. Rev. B: Condens. Matter Mater. Phys.* **2015**, *92*, 155412.
(35) Martin-Jimenez, D.; Chacon, E.; Tarazona, P.; Garcia, R. Atomically Resolved Three-Dimensional Structures of Electrolyte Aqueous Solutions near a Solid Surface. *Nat. Commun.* **2016**, *7*, 12164.
(36) Söngen, H.; Marutschke, C.; Spijker, P.; Holmgren, E.; Hermes, I.; Bechstein, R.; Klassen, S.; Tracey, J.; Foster, A. S.; Kühnle, A. Chemical Identification at the Solid-Liquid Interface. *Langmuir* **2017**, *33*, 125−129.
(37) Geissbühler, P.; Fenter, P.; DiMasi, E.; Srajer, G.; Sorensen, L. B.; Sturchio, N. C. Three-Dimensional Structure of the Calcite-Water Interface by Surface X-Ray Scattering. *Surf. Sci.* **2004**, *573*, 191−203.
(38) Heberling, F.; Trainor, T. P.; Lützenkirchen, J.; Eng, P.; Denecke, M. A.; Bosbach, D. Structure and Reactivity of the Calcite−Water Interface. *J. Colloid Interface Sci.* **2011**, *354*, 843−857.
(39) Fenter, P.; Kerisit, S.; Raiteri, P.; Gale, J. D. Is the Calcite−Water Interface Understood? Direct Comparisons of Molecular Dynamics Simulations with Specular X-Ray Reflectivity Data. *J. Phys. Chem. C* **2013**, *117*, 5028−5042.
(40) Heberling, F.; et al. Reactivity of the Calcite-Water Interface, from Molecular Scale Processes to Geochemical Engineering. *Appl. Geochem.* **2014**, *45*, 158−190.
(41) Robinson, C.; Mills, H. A. T. The Colloid Chemistry of Dyes: The Aqueous Solutions of Benzopurpurine 4b and Its Isomer Prepared from M-Tolidine. Part I. *Proc. R. Soc. London, Ser. A* **1931**, *131*, 576−595.
(42) McKitterick, C. B.; Erb-Satullo, N. L.; LaRacuente, N. D.; Dickinson, A. J.; Collings, P. J. Aggregation Properties of the Chromonic Liquid Crystal Benzopurpurin 4b. *J. Phys. Chem. B* **2010**, *114*, 1888−1896.
(43) Rode, S. W. A. Optimization of an Atomic Force Microscope and Its Application for Highest-Resolution Imaging in Liquid Environments. Dissertation, Johannes Gutenberg-Universität, Mainz, 2011.
(44) Adam, H.; Rode, S.; Schreiber, M.; Kobayashi, K.; Yamada, H.; Kühnle, A. Photothermal Excitation Setup for a Modified Commercial Atomic Force Microscope. *Rev. Sci. Instrum.* **2014**, *85*, 023703.
(45) Harstad, A. O.; Stipp, S. L. S. Calcite Dissolution: Effects of Trace Cations Naturally Present in Iceland Spar Calcites. *Geochim. Cosmochim. Acta* **2007**, *71*, 56−70.
(46) Plimpton, S. Fast Parallel Algorithms for Short-Range Molecular Dynamics. *J. Comput. Phys.* **1995**, *117*, 1−19.
(47) Tribello, G. A.; Bonomi, M.; Branduardi, D.; Camilloni, C.; Bussi, G. Plumed 2: New Feathers for an Old Bird. *Comput. Phys. Commun.* **2014**, *185*, 604−613.
(48) Wang, J.; Wolf, R. M.; Caldwell, J. W.; Kollman, P. A.; Case, D. A. Development and Testing of a General Amber Force Field. *J. Comput. Chem.* **2004**, *25*, 1157−1174.
(49) Raiteri, P.; Demichelis, R.; Gale, J. D. Thermodynamically Consistent Force Field for Molecular Dynamics Simulations of Alkaline-Earth Carbonates and Their Aqueous Speciation. *J. Phys. Chem. C* **2015**, *119*, 24447−24458.
(50) Kellermeier, M.; Raiteri, P.; Berg, J. K.; Kempter, A.; Gale, J. D.; Gebauer, D. Entropy Drives Calcium Carbonate Ion Association. *ChemPhysChem* **2016**, *17*, 3535−3541.
(51) De La Pierre, M.; Raiteri, P.; Stack, A. G.; Gale, J. D. Uncovering the Atomistic Mechanism for Calcite Step Growth. *Angew. Chem., Int. Ed.* **2017**, *56*, 8464−8467.
(52) Byrne, E. H.; Raiteri, P.; Gale, J. D., Computational Insight into the Calcium-Sulfate Ion Pair Formation. Submitted for publication, 2017.
(53) Wu, Y. J.; Tepper, H. L.; Voth, G. A. Flexible Simple Point-Charge Water Model with Improved Liquid-State Properties. *J. Chem. Phys.* **2006**, *124*, 024503.
(54) Laio, A.; Parrinello, M. Escaping Free-Energy Minima. *Proc. Natl. Acad. Sci. U. S. A.* **2002**, *99*, 12562−12566.
(55) Raiteri, P.; Laio, A.; Gervasio, F. L.; Micheletti, C.; Parrinello, M. Efficient Reconstruction of Complex Free Energy Landscapes by Multiple Walkers Metadynamics. *J. Phys. Chem. B* **2006**, *110*, 3533−3539.
(56) Barducci, A.; Bussi, G.; Parrinello, M. Well-Tempered Metadynamics: A Smoothly Converging and Tunable Free-Energy Method. *Phys. Rev. Lett.* **2008**, *100*, 020603.
(57) Park, H.-S.; Kang, S.-W.; Tortora, L.; Nastishin, Y.; Finotello, D.; Kumar, S.; Lavrentovich, O. D. Self-Assembly of Lyotropic Chromonic Liquid Crystal Sunset Yellow and Effects of Ionic Additives. *J. Phys. Chem. B* **2008**, *112*, 16307−16319.
(58) Dickinson, A. J.; LaRacuente, N. D.; McKitterick, C. B.; Collings, P. J. Aggregate Structure and Free Energy Changes in Chromonic Liquid Crystals. *Mol. Cryst. Liq. Cryst.* **2009**, *509*, 9−20.
(59) Ostapenko, T.; Nastishin, Y. A.; Collings, P. J.; Sprunt, S. N.; Lavrentovich, O. D.; Gleeson, J. T. Aggregation, Pretransitional Behavior, and Optical Properties in the Isotropic Phase of Lyotropic Chromonic Liquid Crystals Studied in High Magnetic Fields. *Soft Matter* **2013**, *9*, 9487−9498.
(60) Agra-Kooijman, D. M.; Singh, G.; Lorenz, A.; Collings, P. J.; Kitzerow, H.-S.; Kumar, S. Columnar Molecular Aggregation in the Aqueous Solutions of Disodium Cromoglycate. *Phys. Rev. E* **2014**, *89*, 062504.
(61) Xiao, W.; Hu, C.; Carter, D. J.; Nichols, S.; Ward, M. D.; Raiteri, P.; Rohl, A. L.; Kahr, B. Structural Correspondence of Solution, Liquid Crystal, and Crystalline Phases of the Chromonic Mesogen Sunset Yellow. *Cryst. Growth Des.* **2014**, *14*, 4166−4176.
(62) MacKintosh, F. C.; Safran, S. A.; Pincus, P. A. Self-Assembly of Linear Aggregates: The Effect of Electrostatics on Growth. *Europhys. Lett.* **1990**, *12*, 697.
(63) Raiteri, P.; Gale, J. D.; Quigley, D.; Rodger, P. M. Derivation of an Accurate Force-Field for Simulating the Growth of Calcium Carbonate from Aqueous Solution: A New Model for the Calcite-Water Interface. *J. Phys. Chem. C* **2010**, *114*, 5997−6010.
(64) Rahe, P.; Schütte, J.; Kühnle, A. Nc-Afm Contrast Formation on the Calcite (1014). *J. Phys.: Condens. Matter* **2012**, *24*, 084006.
(65) Cheng, L.; Fenter, P.; Nagy, K. L.; Schlegel, M. L.; Sturchio, N. C. Molecular-Scale Density Oscillations in Water Adjacent to a Mica Surface. *Phys. Rev. Lett.* **2001**, *87*, 156103.
(66) Wang, J.; Kalinichev, A. G.; Kirkpatrick, R. J.; Cygan, R. T. Structure, Energetics, and Dynamics of Water Adsorbed on the Muscovite (001) Surface: A Molecular Dynamics Simulation. *J. Phys. Chem. B* **2005**, *109*, 15893−15905.
(67) Reischl, B.; Watkins, M.; Foster, A. S. Free Energy Approaches for Modeling Atomic Force Microscopy in Liquids. *J. Chem. Theory Comput.* **2013**, *9*, 600−608.

DOI: 10.1021/acs.jpcc.7b09825
J. Phys. Chem. C 2017, 121, 24144−24151